Supplementary Materials
Sensitivity of source sediment fingerprinting modelling to tracer selection methods.

1. Laboratory analysis

1.0.1. Organic Matter

In the Hayama lake catchment, sediment and soils were found not to contain carbonate minerals, and all the carbon associated with particulate matter is organic in nature (Huon et al., 2018). Total organic carbon (TOC) and total nitrogen (TN) elemental concentrations and isotopes (δ^{13}C and δ^{15}N) were determined by a combustion method using a continuous flow elementary analyser (Elementar VarioPyro cube) coupled with an Isotope Ratio Mass Spectrometer (EA-IRMS) (Micromass Isoprime) at the Institute of Ecology and Environmental Sciences (iEES Paris) in France. A first analysis run was conducted to measure TOC concentration together with a set of tyrosine standards (Coplen et al., 1983). The second analysis run was dedicated to measure TN concentration after sample weight optimisation from TOC results. For combustion, oxygen was injected during 70 s (30 mLmin^{-1}) at 850 $^\circ C$ for reduction and the combustion furnace at 1120 $^\circ C$ (Agnihotri et al., 2014). The analytical precision was assessed with repeated analyses of a tyrosine intern standard ($n = 51$), calibrated against international reference standards (Girardin & Mariotti, 1991). The analysis of these properties in source material is described in details in the study of Laceby et al. (2016). To evaluate whether the samples are composed of terrestrial or freshwater-originating material the distribution of sample values was plotted in a δ^{13}C versus TOC/TN diagram and compared to the thresholds reported in Lamb et al. (2006) (Fig. S1).
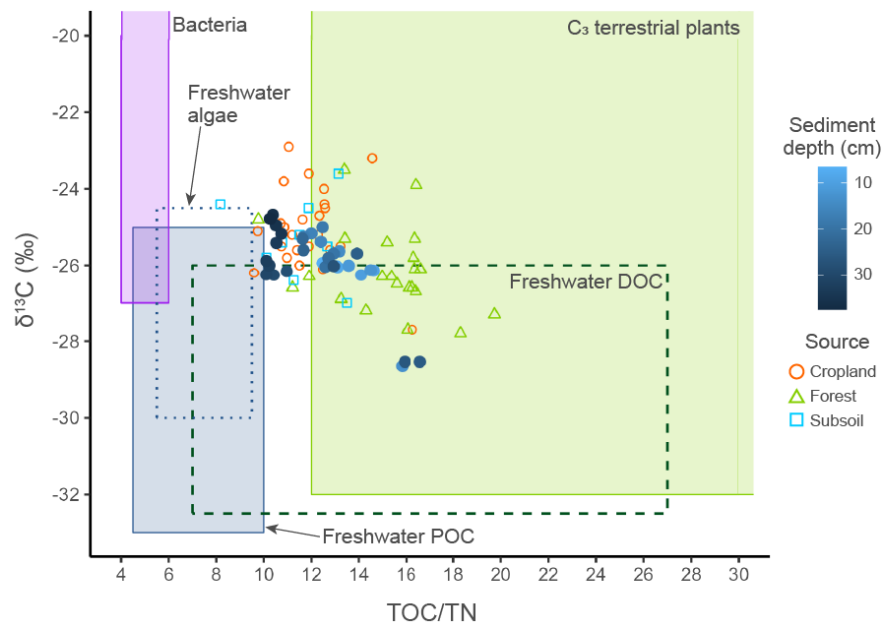

Figure S1: Sediment core and source samples δ^{13}C and TOC/N and typical ranges for organic inputs to lacustrine environments (thresholds from (Lamb et al., 2006)).

1.0.2. Geochemistry

Elemental geochemistry was determined using X-ray fluorescence (XRF) (Malvern Panalytical, ED-XRF Epsilon 4). A total of 17 elemental concentrations were measured (Al, Ca, Co, Cr, Cu, Fe, K, Mg, Mn,

Ni, Pb, Rb, Si, Sr, Ti, Zn, and Zr). Measurements were conducted in containers covered with a 3.6 µm thin Mylar film (Chemplex, Mylar Thin-Film cat. no. 157) with a 10 mm exposure surface. A minimum of 0.1 g of material was analysed. To consider the potential heterogeneity within a sample, three replicate measurements were made, and the mean value of these replicates was calculated. To assess the accuracy of the measurements, a standard (JMS-1, sediment from the Tokyo Bay (Terashima et al., 2002)) was measured every seven samples ($n = 38$) and the accuracy of the measured batch was determined based on the calculation of the Root Mean Square Errors (RMSE).

1.0.3. Visible colorimetry

Visible colorimetry was measured using a portable diffuse reflectance spectrophotometer, Kanonica Minolta CM-700d, set on a 3 mm target radius. Samples were measured in a plastic zip bag. In order to for account potential heterogeneities within a sample, three measurements were made at different locations on the bag. The spectrophotometer was calibrated at the start of each set of measurements with a zero (black) and white standards. Measurements were conducted according to the D65 illuminance standard, 10° angle observer and excluding the specular component. The spectral reflectance (in %) was measured from 360 nm to 740 nm with a 10 nm resolution (30 wavelength classes). Raw data was processed using the colour data software CM-S100w SpectraMagic NX (Kanonica Minolta, 2022). Colour parameters within the Cartesian coordinate systems CIE Lab (1976) (i.e. L*, a* and b*) (ISO 11664-4:2008) and CIE LCh (i.e. C* and h) were exported. The CIE LCh is a vector representation of the CIE Lab (1976). C and h are derived from a* and b* parameters. Within the CIE Lab system: L* is the lightness of the colour, from black (0) to white (100), a* is the position between green to red (negative values are associated with green and positives with red), b* is the position between blue and yellow (negative values are associated with blue and positive values with yellow). Within the CIE LCh system: C* is the chroma (positive values are associated to brighter colors and negative values to duller colors) and h is the hue angle (in °) in the CIE Lab color wheel.

The Q7/4 ratio as defined by Debret et al. (2011) was calculated as the ratio between 700 nm and 400 nm reflectance values. This ratio provides a numerical description of the reflectance spectrum general slope.

The oxy-hydroxide geothite (α-FeOOH) soil richness can be determined using visible diffuse reflectance spectra (Kosmas et al., 1984; Balsam et al., 2004; Hao et al., 2009; Torrent et al., 2007) and its peaks values at 445 nm and 525 nm were calculated from the first derivative reflectance spectrum Debret et al. (2011). In our case the geothite concentration was not aimed, only the relative abundance among our samples in order to differentiate between them. For each replicate of the measurements and for each sample, the first derivative reflectance spectrum was calculated and smoothed with a Savitzky-Golay filter using the savitzkyGolay function (differentiation order = 1, polynomial order = 3, window size = 5 (eq. 50 nm)) from R package prospectr (Stevens & Ramirez-Lopez, 2022) (Wadoux et al., 2021). Then the mean per sample and the standard deviation were calculated. From the first derivative of reflectance, two geothite peaks were calculated: first, the 445 nm peak value was calculated as the mean of values at 440 and 450 nm, and the 525 nm peak as the mean of those at 520 and 530 nm (Debret et al., 2011).

The remission function was calculated from the reflectance spectrum: $f(R) = (1 - R)^2$ according to the Kubelka-Munk relationship (Scheinost et al., 1998). Then, the second derivative was calculated and the spectrum was smoothed with a Savitzky-Golay filter using the savitzkyGolay function (differentiation order = 2, polynomial order = 3, window size = 5). From the second derivative of remission function spectrum, the iron oxide-associated parameters A1, A2, A3 and the goethite proportion within iron oxides (Gt) (Tiecher et al., 2015). The A1 and A2 peaks are associated with goethite and the A3 peak is associated with hematite, and all peaks were calculated as the amplitude between each maximum and minimum bands. Thus, A1 is the difference between 450 and 420 nm, A2 is the difference between 510 and 480 nm and A3 is the difference between 575 (as the mean of 570 and 580 nm) and 535 nm (as the mean of 530 and 540 nm) and Gt is calculated as the ratio of A1/(A1+A3).

1.0.4. Tracers Linear Pearson correlations

Table I: Selected tracers Pearson correlation coefficients. · = correlation with significance test p-value lower than 0.05.

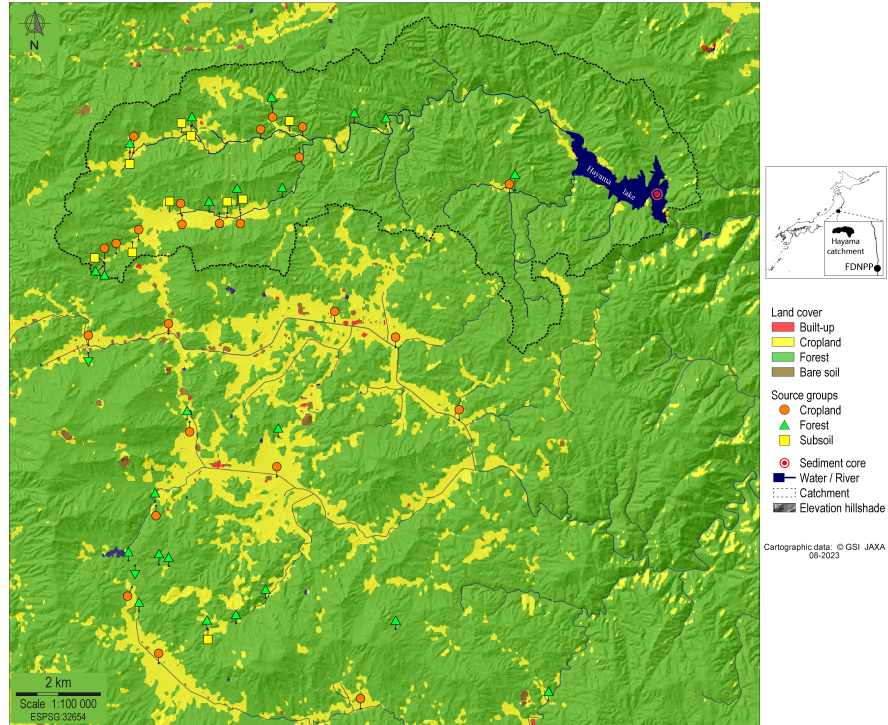|	TOC	TN	Al	Ca	K	Si	Sr	Zn	Zr	L*	a*	b*	C*	h	A1	A2	Gt	Q7/4
TN	0.97																	
Al	-0.76	-0.83																
Ca	0.13	0.21	-0.52															
K	-0.33	-0.37	0.56	-0.50														
Si	-0.47	-0.53	0.51	-0.41	0.47													
Sr	0.05	0.12	-0.49	0.87	-0.53	-0.37												
Zn	0.06	0.20	-0.28	0.47	-0.39	-0.53	0.23											
Zr	·	-0.27	0.47	-0.43	0.71	0.24	-0.48	-0.19										
L*	-0.71	-0.77	0.83	-0.56	0.65	0.53	-0.50	-0.37	0.53									
a*	-0.29	-0.43	0.66	-0.63	0.29	0.39	-0.53	-0.43	0.37	0.61								
b*	-0.63	-0.72	0.75	-0.49	0.20	0.45	-0.38	-0.32	·	0.68	0.79							
C*	-0.61	-0.71	0.75	-0.52	0.21	0.45	-0.40	-0.34	0.17	0.69	0.83	1.00						
h	·	·	·	·	·	·	0.30	·	-0.35	·	·	·	·	·				
A1	·	·	·	·	-0.56	·	0.36	·	-0.55	·	·	·	·	0.55				
A2	-0.27	-0.27	·	·	·	·	·	·	·	·	0.41	0.58	0.58	·	0.77			
Gt	·	·	-0.32	0.55	-0.23	-0.21	0.52	0.33	-0.37	-0.30	-0.68	-0.28	-0.33	0.64	·	·		
Q7/4	-0.49	-0.54	0.47	·	·	0.17	·	·	·	0.35	0.52	0.83	0.81	·	0.76	0.82	·	
G_{525}	-0.59	-0.68	0.80	-0.57	0.44	0.53	-0.50	-0.42	0.33	0.83	0.78	0.89	0.89	·	·	0.44	-0.35	0.64

1.0.5. Complementary maps

Figure S2: Map of the main land uses in the study area over the 2014-2016 period with location of source samples and the sediment core (cartographic data: GSI and JAXA). FDNPP: Fukushima Dai-ichi Nuclear power plant.
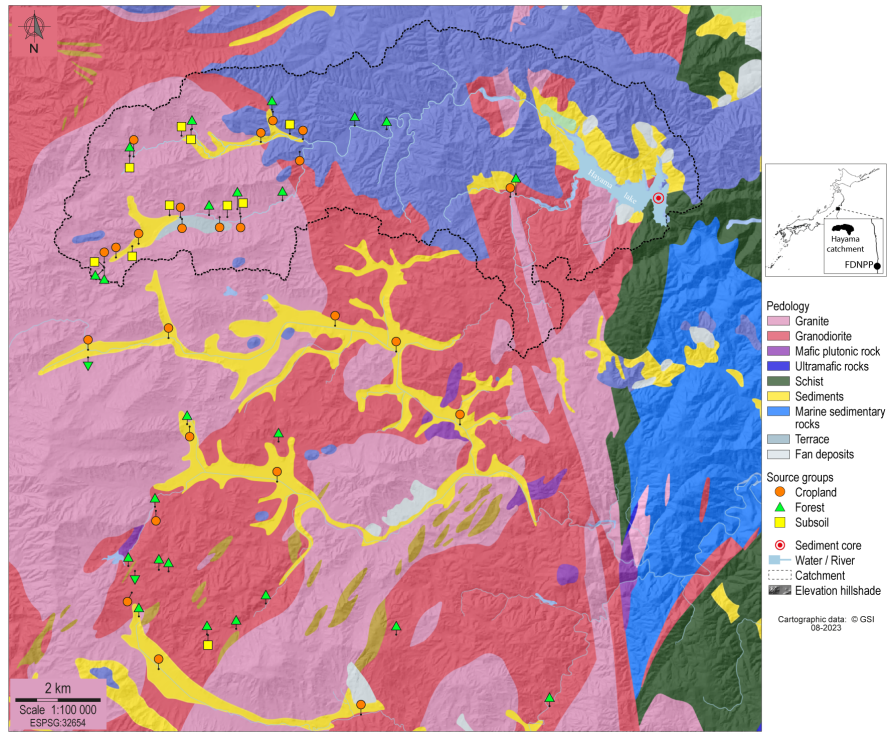
Figure S3: Map of the mean geology types in the study area with location of source samples and the sediment core (cartographic data: GSI). FDNPP: Fukushima Dai-ichi Nuclear power plant.
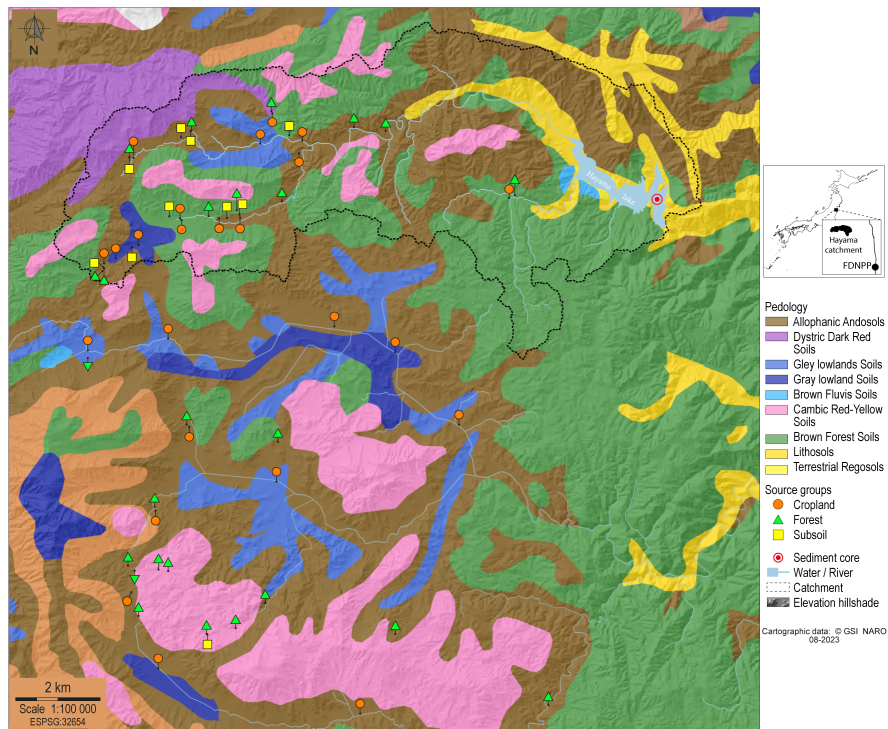

Figure S4: Map of the main soil types in the study area with location of source samples and the sediment core (cartographic data: GSI and NARO). FDNPP: Fukushima Dai-ichi Nuclear power plant.

References

Agnihotri, R., Kumar, R., Prasad, M., Sharma, C., Bhatia, S., & Arya, B. (2014). Experimental setup and standardization of a continuous flow stable isotope mass spectrometer for measuring stable isotopes of carbon, nitrogen and sulfur in environmental samples. *Mapan*, *29*, 195–205. doi:https://doi.org/10.1007/s12647-014-0099-8.

Balsam, W., Ji, J., & Chen, J. (2004). Climatic interpretation of the luochuan and lingtai loess sections, china, based on changing iron oxide mineralogy and magnetic susceptibility. *Earth and Planetary Science Letters*, *223*, 335–348.

Coplen, T. B., Kendall, C., & Hopple, J. (1983). Comparison of stable isotope reference samples. *Nature*, *302*, 236–238. doi:http://dx.doi.org/10.1038/302236a0.

Debret, M., Sebag, D., Desmet, M., Balsam, W., Copard, Y., Mourier, B., Susperrigui, A.-S., Arnaud, F., Bentaleb, I., Chapron, E. et al. (2011). Spectrocolorimetric interpretation of sedimentary dynamics: The new "q7/4 diagram". *Earth-Science Reviews*, *109*, 1–19. doi:https://doi.org/10.1016/j.earscirev.2011.07.002.

Girardin, C., & Mariotti, A. (1991). Analyse isotopique du 13c en abondance naturelle dans le carbone organique: un système automatique avec robot préparateur. *Cah ORSTOM Ser Pedofil*, *26*, 371–380.

Hao, Q., Oldfield, F., Bloemendal, J., Torrent, J., & Guo, Z. (2009). The record of changing hematite and goethite accumulation over the past 22 myr on the chinese loess plateau from magnetic measurements and diffuse reflectance spectroscopy. *Journal of Geophysical Research: Solid Earth*, *114*.

Huon, S., Hayashi, S., Laceby, J. P., Tsuji, H., Onda, Y., & Evrard, O. (2018). Source dynamics of radiocesium-contaminated particulate matter deposited in an agricultural water reservoir after the fukushima nuclear accident. *Science of the Total Environment*, *612*, 1079–1090. doi:https://doi.org/10.1016/j.scitotenv.2017.07.205.

ISO 11664-4:2008 (2008). *Colorimetry — Part 4: CIE 1976 L*a*b* Colour space*. Standard CIE International Commission on Illumination Geneva, CH.

Kanonica Minolta (2022). *QCM-S100w SpectraMagic NX*. Kanonica Minolta. URL: https://www.konicaminolta.com/instruments/download/software/color/smnx/index.html version 3.31.0000.

Kosmas, C., Curi, N., Bryant, R., & Franzmeier, D. (1984). Characterization of iron oxide minerals by second-derivative visible spectroscopy. *Soil Science Society of America Journal*, *48*, 401–405.

Laceby, J. P., Huon, S., Onda, Y., Vaury, V., & Evrard, O. (2016). Do forests represent a long-term source of contaminated particulate matter in the fukushima prefecture? *Journal of Environmental Management*, *183*, 742–753. doi:https://doi.org/10.1016/j.jenvman.2016.09.020.

Lamb, A. L., Wilson, G. P., & Leng, M. J. (2006). A review of coastal palaeoclimate and relative sea-level reconstructions using δ13c and c/n ratios in organic material. *Earth-Science Reviews*, *75*, 29–57. doi:https://doi.org/10.1016/j.earscirev.2005.10.003.

Scheinost, A., Chavernas, A., Barrón, V., & Torrent, J. (1998). Use and limitations of second-derivative diffuse reflectance spectroscopy in the visible to near-infrared range to identify and quantify fe oxide minerals in soils. *Clays and Clay Minerals*, *46*, 528–536. doi:http://dx.doi.org/10.1346/CCMN.1998.0460506.

Stevens, A., & Ramirez-Lopez, L. (2022). *An introduction to the prospectr package*. R package version 0.2.5.

Terashima, S., Imai, N., Taniguchi, M., Okai, T., & Nishimura, A. (2002). The Preparation and Preliminary Characterisation of Four New Geological Survey of Japan Geochemical Reference Materials: Soils, JSO-1 and JSO-2; and Marine Sediments, JMS-1 and JMS-2, . *26*, 85–94. URL: https://onlinelibrary.wiley.com/doi/10.1111/j.1751-908X.2002.tb00626. doi:10.1111/j.1751-908X.2002.tb00626.

Tiecher, T., Caner, L., Minella, J. P. G., & dos Santos, D. R. (2015). Combining visible-based-color parameters and geochemical tracers to improve sediment source discrimination and apportionment. *Science of the Total Environment*, *527*, 135–149. doi:https://doi.org/10.1016/j.scitotenv.2015.04.103.

Torrent, J., Liu, Q., Bloemendal, J., & Barrón, V. (2007). Magnetic enhancement and iron oxides in the upper luochuan loess–paleosol sequence, chinese loess plateau. *Soil Science Society of America Journal*, *71*, 1570–1578.

Wadoux, A. M. J.-C., Malone, B., Minasny, B., Fajardo, M., & McBratney, A. B. (2021). *Soil Spectral Inference with R: Analysing Digital Soil Spectra Using the R Programming Environment*. Springer Nature, Cham.